A Novel Modulation Method Based on Model Prediction Control With Significantly Reduced Switching Loss and Current Zero-Crossing Distortion for Vienna Rectifier

Qingyan Zhang, Fang Liu, *Senior Member, IEEE*, Weidong Jiang, *Member, IEEE*, Jinping Wang, *Member, IEEE*, and Yimin Yue

***Abstract*—Finite control set model predictive control (FCS-MPC) is widely used in rectifiers due to its fast response. When there are multiple control objectives, the optimal switching sequence is selected by minimizing the cost function with weighting factors. However, the reduction of current ripple caused by output error and switching loss is in conflict to a certain extent for FCS-MPC. In addition, when multiple objectives are controlled, the selection of weighting factor is a serious challenge. Therefore, a modulation method based on continuous control set model predictive control is proposed in this article. Two phases are clamped and one phase is modulated, which not only can significantly reduce the switching loss without increasing the computational burden, but also can control the neutral point voltage without using weighting factors. In addition, when the proposed method is adopted, current zero-crossing distortion can be suppressed over the full range of modulation index. The effectiveness of the proposed method is verified by simulation and experimental results.**

***Index Terms*—Current zero-crossing distortion, model predictive control (MPC), switching loss, Vienna rectifier.**

I. Introduction

VIENNA rectifier is a three-phase three-level topology with unidirectional energy flow, whose outer and inner tubes are diodes and IGBTs with antiparallel diodes, respectively. The switching of the current path depends on the ON–OFF of the IGBT, which means that Vienna rectifier has the advantages of high power density, high reliability and eliminating the switching dead zone [1], [2]. Therefore, Vienna rectifiers are widely used in wind turbines [3], [4], communication power sources [5], and electric vehicles [6], [7].

Manuscript received 14 February 2022; revised 19 May 2022 and 5 August 2022; accepted 28 September 2022. Date of publication 12 October 2022; date of current version 18 November 2022. This work was supported by the National Natural Science Foundation of China under Grant 51907044 and Grant 52077050. Recommended for publication by Associate Editor J. Biela. *(Corresponding author: Fang Liu.)*

The authors are with the School of Electrical Engineering and automation, Hefei University of Technology, Hefei 230009, China (e-mail: zqyzqy117@163.com; fragcelau@hfut.edu.cn; ahjwd@163.com; waupter919@163.com; 206005494@qq.com).

Color versions of one or more figures in this article are available at https://doi.org/10.1109/TPEL.2022.3213795.

Digital Object Identifier 10.1109/TPEL.2022.3213795

The following requirements need to be met during the high-performance operation for Vienna rectifier: 1) The total harmonic distortion (THD) of the current is low. 2) The switching loss is as low as possible. 3) The neutral point voltage balance can be achieved, or the fluctuation of the neutral point voltage is controlled within a small range. In order to meet the abovementioned requirements, many control methods have been proposed. The most common control method is the double closed-loop control based on the *dq* synchronous rotating coordinate system [8], which has good control performance and is easy to implement. In order to improve the current response speed, hysteresis control was introduced into the Vienna rectifier [9], but the current THD of the hysteresis control is high. The method of using proportional resonance controller was proposed in [5], which can directly track the three-phase ac current in the three-phase static coordinate system. However, the controller is easy to oscillate, and the parameter design is very difficult in the actual system. In addition, the existing control methods include deadbeat control [10], sliding mode control [11], and so on.

In recent years, with the rapid development of microprocessors, model predictive control (MPC) has become more and more popular in power electronics. MPC is a multiobjective hybrid control method including nonlinear constraints, which has the advantages of fast response and strong robustness against disturbances [12]. MPC can be classified into finite control set MPC (FCS-MPC) and continuous control set MPC (CCS-MPC). In FCS-MPC, finite number of candidate sets are determined through certain constraints, and the switch sequence that minimizes the cost function is selected from the candidate sets. When traditional FCS-MPC is adopted, only one basic voltage vector is selected in each control cycle, the maximum output error of the voltage can reach 50%, and the current THD is relatively high. In order to reduce the output error in each control cycle, a method to expand the candidate sets with virtual vectors synthesized by basic voltage vectors was proposed in [13]. However, this method has a large computational burden and increases switching actions in a control cycle. A method that combines the advantages of space vector modulation (SVM) and FCS-MPC was proposed in [14], which reduced the current THD

and computational burden. However, the reduction of switching loss is not considered.

In fact, the performance of FCS-MPC mainly depends on the number of candidate vectors and the selection principle [15]. In order to reduce the current THD, the vectors selected by FCS-MPC should have a lower cost function. In order to reduce the switching loss, the vector selected by FCS-MPC should have fewer switching actions. The more candidate vectors of FCS-MPC, the greater the possibility it is to obtain a smaller cost function, but the computational burden is increased [16]. The vectors only located at the edge of the sector can be selected as the candidate vector, which is represented by [13]. The vectors located inside the sector can also be selected as candidate vectors, which is represented by [14]. If the vectors only at the edge of the sector are selected as the candidate vectors, the candidate vectors are not evenly distributed in the space vector diagram, and its cost function may be high, resulting in large current THD. However, the vectors at the edge of the sector can be realized by modulating only one phase, the switching loss is low. If the vectors inside the sector are selected as the candidate vectors, the candidate vectors can be evenly distributed in the space vector diagram and the cost function is smaller than the former, and the current THD is lower. However, the vectors inside the sector must be realized by modulating three phases at the same time, the switching loss is higher. In general, when FCS-MPC is used, the reduction of current THD and switching loss is in conflict to a certain extent. In order to reduce current THD and switching loss at the same time, a discontinuous pulsewidth modulation suitable for Vienna rectifiers was proposed in [15] and [16]. In [15], the clamping mode was selected according to the current, and the current zero-crossing distortion can be reduced. However, the clamping interval of Vienna rectifier is limited, and the switching loss cannot be reduced to less than 50%. In addition, the suppression effect on current zero-crossing distortion is not obvious when the modulation index is high.

The neutral point voltage balance is a key object for three-level rectifiers. Excessive dc offset will lead to overvoltage of the power device and even lead to danger [17]. Taking the neutral point voltage as a part of the cost function was proposed in [18], which achieved multiobjective control by adjusting the weighting factor. The control performance of the system for different control objectives can be quickly changed by adjusting the weight factor, which is simple and superior. However, in actual control system, the choice of weighting factor is a challenge. To eliminate the influence of the weighting factor, the method to control the neutral point voltage by adjusting the duty ratio of the redundant small vectors was proposed in [19]. When the basic voltage vector that minimizes the cost function does not contain small vectors, this method will be invalid. The idea of virtual space vector modulation was introduced into MPC in [20]. The basic voltage vectors that affect the neutral point voltage is removed from the candidate sets, only the basic voltage vectors and the expanded virtual vectors that do not affect the neutral point voltage are retained. However, the number of switching actions is relatively large as well as the burden of online calculation.

In this article, the voltage cost function is used to replace the current cost function, and the reference voltage vector ($\boldsymbol{u}_{ref}$) used to accurately track the current is calculated. In fact, $\boldsymbol{u}_{ref}$ may be located at any position in the space vector diagram, and it may not be accurately synthesized by any modulation method due to the limitation of Vienna rectifier. Therefore, the main contributions of this article are as follows.

1) All vectors at the edge of the triangle are selected as candidate vectors, and the vector closest to $\boldsymbol{u}_{ref}$ among the candidate vectors is selected as the output vector, which further reduces the output error and the current quality compared to the method in [13]. Moreover, in terms of reducing switching loss, the method proposed in this article has the same characteristic with FCS-MPC, which only selects the vectors at the edge of the triangle as the candidate vector.
2) In (1), if $\boldsymbol{u}_{ref}$ cannot be accurately synthesized by any modulation method, the method based on the principle of minimum synthesis error is given in this article, which is obviously better than the other existing methods in terms of current zero-crossing distortion caused by the fact that $\boldsymbol{u}_{ref}$ cannot be accurately synthesized.
3) Based on the proposed method, the three-phase output voltage is derived directly, which can greatly simplify the calculation.
4) The active neutral point voltage control method suitable for the proposed method is also given.

In Section II, the basic principle of Vienna rectifier is introduced, and the causes of current zero-crossing distortion are briefly analyzed. In Section III, MPC methods based on minimizing the current error and based on minimizing the output voltage error are, respectively, introduced. In Section IV, the principle and the neutral point voltage control method suitable for the proposed method are introduced. In Sections V and VI, SVPWM without current zero-crossing distortion processing, SVPWM with current zero-crossing distortion processing, CB-DSVM proposed in [15] and the method proposed in this article are compared in terms of switching loss, efficiency and current THD. Simulation and experimental results verify the feasibility and superiority of the method proposed in this article.

II. Analysis of Vienna Rectifier

The topology of Vienna rectifier is shown in Fig. 1, where L_s and R_s are the filter inductor and its equivalent series resistance, R_L is the load, e_x ($x = a, b, c$) is the three-phase grid voltage, u_x is the three-phase output voltage of the rectifier, i_x is the three-phase input current, and C_1 and C_2 are the upper and lower capacitors of the dc side. The dc-link voltage is $u_{\rm dc}$, and $u_{C1} = u_{C2} = u_{\rm dc}/2$ when the capacitor voltages are balanced.

The switching function S_x ($x = a, b, c$) represents the state of the switch devices. When the switch devices are on, $S_x = 1$; when the switch devices are off, $S_x = 0$. When $S_x = 1$, whether the current is positive or negative, the output of this phase is connected to neutral point O, and the state is defined as level 0. When $S_x = 0$, if the current is positive, the output of this phase

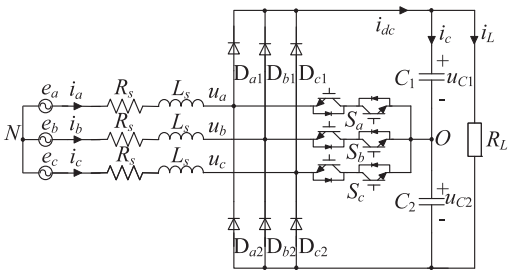

Fig. 1. Topology of Vienna rectifier.

TABLE I
OUTPUT LEVEL OF VIENNA RECTIFIER

I. Sign of current	S_x	Output level of x-phase
i_x>0	1	0
	0	1
i_x<0	1	0
	0	-1

is connected to the positive bus through the diode D_{x1}, and the state is defined as level 1; if the current is negative, the output of this phase is connected to the negative bus through the diode D_{x2}, and the state is defined as the level -1. The relationship between S_x and the output level of x-phase is shown in Table I

$$\boldsymbol{u} = u_\alpha + ju_\beta = \sqrt{\frac{2}{3}}\left(u_a + u_b e^{j\frac{2\pi}{3}} + u_c e^{j\frac{4\pi}{3}}\right). \quad (1)$$

Substituting the three-phase output voltage of Vienna rectifier into (1), 27 basic voltage vectors can be obtained. Each vector can be represented by a three-dimensional ordered array, as shown in Fig. 2. For example, [1, 0, 0] means that phase A outputs level 1, phases B and C output level 0. There are no vectors [1, 1, 1] and [-1, -1, -1] in Vienna rectifier, and 25 basic voltage vectors are available. According to the length of the basic voltage vectors, basic voltage vectors can be classified into 6 large vectors, 6 medium vectors, 12 small vectors, and 1 zero vector. The length of the small vector is defined as 1 in this article. Substituting the reference output voltage and current into (1), the reference voltage vector ($\boldsymbol{u_{ref}}$) and current vector ($\boldsymbol{i}$) can be obtained. According to the sign of the three-phase current, it can be classified into 6 sectors (I, …, VI). For example, when i_a>0, i_b<0, and i_c<0 (current state I), the current vector $\boldsymbol{i}$ is located in the Sector I. Phase A is allowed to output level 1 and 0, phase B and C are allowed to output level 0 and -1. As shown in Fig. 2, when $\boldsymbol{i}$ is in the current state I, the basic voltage vectors that can be used to synthesize $\boldsymbol{u_{ref}}$ forms a small hexagon, denoted as Hexagon I.

Vienna rectifiers usually operate at the unity power factor on the grid side. Therefore, $\boldsymbol{u_{ref}}$ lags behind $\boldsymbol{i}$ and the angle is usually less than $\pi/6$. Therefore, when the current is in current state I, $\boldsymbol{u_{ref}}$ may be located in the triangle F3, as shown in Fig. 2. Among the three vectors corresponding to the three vertices of the triangle F3, only [0, -1, 0] and [1, -1, 0] can be realized. [1, -1, 1] cannot be realized and will be replaced by the vector [1, 1, -1], which causes current zero-crossing distortion of Vienna rectifier.

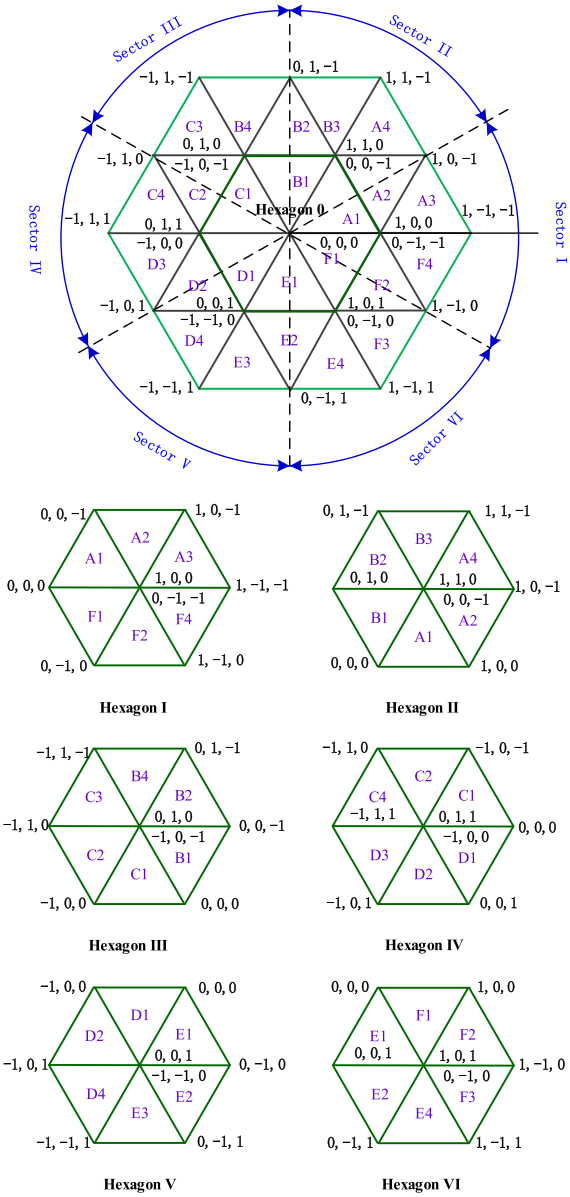

Fig. 2. Decomposition of the space vector diagram of the Vienna rectifier.

Once this case happens, the current zero-crossing distortion cannot be eliminated and can only be reduced by modulation methods. The method to minimize the current zero-crossing distortion will be introduced in Section IV.

III. MODEL PREDICTIVE CONTROL

A. MPC Based on Minimizing Current Error

The voltage drop across the equivalent series resistor of the filter inductor can be ignored. Then, the continuous mathematical model of Vienna rectifier under the $\alpha\beta$ coordinate can be expressed as

$$L_s \frac{di_{\alpha\beta}}{dt} = e_{\alpha\beta} - u_{\alpha\beta}. \quad (2)$$

In one control cycle, using Euler difference method to discretize (2), and it yields

$$L_s\frac{i_{\alpha\beta}(n+1)-i_{\alpha\beta}(n)}{T_s}=e_{\alpha\beta}(n+1)-u_{\alpha\beta}(n+1) \quad (3)$$

where n and $n+1$ represent the current control cycle and the next control cycle, respectively. However, there are disturbances and digital delays in actual systems. In terms of disturbances and digital delay compensation, the adopted method is the same as that in [22]. The predicted current can be expressed as

$$\tilde{i}_{\alpha\beta,k}(n+1)=\frac{T_S}{L_s}[e_{\alpha\beta,k}(n+1)-\tilde{u}_{\alpha\beta,k}(n+1)]+i_{\alpha\beta}(n) \quad (4)$$

where $\tilde{u}_{\alpha\beta,k}(n+1)$ represents the voltage of the kth basic voltage vector in the candidate sets under the $\alpha\beta$ coordinate. $\tilde{i}_{\alpha\beta,k}(n+1)$ represents the current when the kth basic voltage vector is modulated.

The current error generated by the kth voltage vector can be expressed as

$$g_{i,k}=\left[i_{\alpha,ref}(n+1)-\tilde{i}_{\alpha,k}(n+1)\right]^2+\left[i_{\beta,ref}(n+1)-\tilde{i}_{\beta,k}(n+1)\right]^2. \quad (5)$$

Assuming that the number of candidate basic voltage vectors is j. It is necessary to make $k=1,\ \ldots, j$ in sequence. Then, the current error generated by each basic voltage vector modulation can be calculated. Finally, the basic voltage vector that can minimizes the current error should be selected for modulation.

B. MPC Based on Minimizing Voltage Error

Equation (5) is the basis for judging the performance of each basic voltage vector, and the number of (5) cannot be reduced. In order to reduce the computational burden, the number of (4) needs to be reduced.

Equation (3) cab be rewritten as

$$u_{\alpha\beta,ref}(n+1)=e_{\alpha\beta}(n+1)-L_s\frac{i_{\alpha\beta,ref}(n+1)-i_{\alpha\beta}(n)}{T_s}. \quad (6)$$

The kth basic voltage vector is substituted into (6), and it yields

$$\tilde{u}_{\alpha\beta,k}(n+1)-u_{\alpha\beta,ref}(n+1)+u_{\alpha\beta,ref}(n+1)=e_{\alpha\beta}(n+1)-\frac{L_s}{T_s}\left[\tilde{i}_{\alpha\beta,k}(n+1)-i_{\alpha\beta}(n)\right]. \quad (7)$$

Substituting (6) into (7), it yields

$$\tilde{u}_{\alpha\beta,k}(n+1)-u_{\alpha\beta,ref}(n+1)=-\frac{L_s}{T_s}\left[\tilde{i}_{\alpha\beta,k}(n+1)-i_{\alpha\beta,ref}(n+1)\right]. \quad (8)$$

Equation (8) is substituted into (5), and $g_{u,k}$ is as follows:

$$\begin{aligned}g_{u,k}&=[u_{\alpha,ref}(n+1)-\tilde{u}_{\alpha,k}(n+1)]^2\\&\quad+[u_{\beta,ref}(n+1)-\tilde{u}_{\beta,k}(n+1)]^2\\&=(T_s/L_s)^2g_{i,k}.\end{aligned} \quad (9)$$

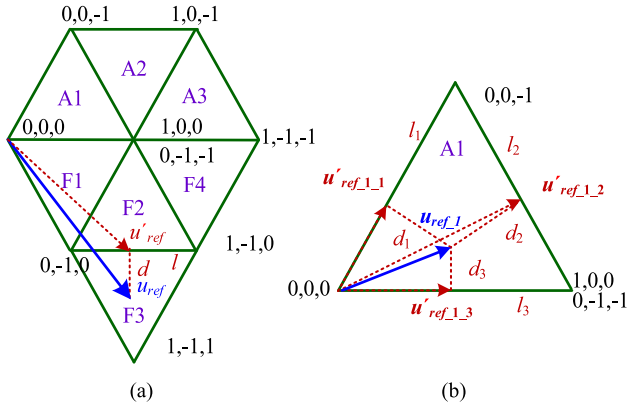

Fig. 3. Modulation vector diagram of the proposed method. (a) Case I. (b) Case II.

Comparing (5) and (9), it can be obtained that the solution to the minimum value of $g_{u,k}$ and $g_{i,k}$ is the same, which means that minimizing the current error and minimizing the voltage error are equivalent.

Assuming that the number of candidate basic voltage vectors is also j. When MPC based on minimizing the voltage error is adopted, the number of calculations for the predicted voltage is 1, and the number of calculations for the error voltage is j. Compared with MPC based on minimizing current error, MPC based on minimizing voltage error reduces the computational burden greatly.

IV. Novel Modulation Method Based on CCS-MPC

A. Principle of the Proposed Method

Based on the analysis in Section I, when $\boldsymbol{i}$ is in current state I, all available basic voltage vectors for Vienna rectifier are located in Hexagon I. The position of $\boldsymbol{u_{ref}}$ can be classified into two cases. One is that $\boldsymbol{u_{ref}}$ is located in the triangle F3, the other is that $\boldsymbol{u_{ref}}$ is located in Hexagon I. From the geometric relationship, the boundary conditions of $\boldsymbol{u_{ref}}$ at Hexagon I and F3 can be expressed as

$$\begin{cases}u_{b,ref}-u_{c,ref}<-u_{dc}, \boldsymbol{u_{ref}}\text{is located in triangle F3}\\ u_{b,ref}-u_{c,ref}\geq -u_{dc}, \boldsymbol{u_{ref}}\text{is located in Hexagon }I\end{cases}. \quad (10)$$

It can be classified into two cases for discussion.

Case I: $\boldsymbol{u_{ref}}$ is located in the triangle F3. Define the line connecting the vectors [0, -1, 0] and [1, -1, 0] as l, the distance from $\boldsymbol{u_{ref}}$ to l is d, and the vector connecting the origin of the coordinates and the foot of perpendicular is $\boldsymbol{u'_{ref}}$. As shown in Fig. 3(a), the vector [1, -1, 1] is not available in this case, and the current zero-crossing distortion cannot be avoided. $\boldsymbol{u'_{ref}}$ is the closest vector to $\boldsymbol{u_{ref}}$ among all available vectors. When $\boldsymbol{u_{ref}}$ is replaced by $\boldsymbol{u'_{ref}}$, the current zero-crossing distortion can be minimized.

In the $\alpha\beta$ coordinate, the line l and the distance d can be expressed as

$$l: u_\beta+\sqrt{3}/2=0,\quad d=-u_\beta-\sqrt{3}/2. \quad (11)$$

The vector $\boldsymbol{u'_{ref}}$ is difficult to solve directly, but it can be expressed as the sum of two vectors

$$\boldsymbol{u'_{ref}} = \boldsymbol{u_{ref}} + \boldsymbol{u_{err}} \tag{12}$$

where $\boldsymbol{u_{err}}$ represents the error vector between $\boldsymbol{u_{ref}}$ and $\boldsymbol{u'_{ref}}\boldsymbol{u'_{err}}$, $\boldsymbol{u_{err}}$ can be expressed as

$$\boldsymbol{u'_{err}} = \frac{d}{\sqrt{3}}[0 \quad 1 \quad -1]^{\mathrm{T}}. \tag{13}$$

Equation (13) is substituted into (12), and the coordinates are transformed to the ABC coordinate system, then the actual output voltage of phase ABC can be expressed as

$$\begin{bmatrix} u'_{a,ref} \\ u'_{b,ref} \\ u'_{c,ref} \end{bmatrix} = \begin{bmatrix} u_{a,ref} \\ (u_{b,ref} + u_{c,ref} - u_{dc})/2 \\ (u_{b,ref} + u_{c,ref} + u_{dc})/2 \end{bmatrix}. \tag{14}$$

In order to reduce switching loss, the zero sequence voltage can be injected to clamp the output levels of phase B and C to level -1 and 0, respectively. The final actual output voltage can be expressed as

$$[u'_{a,ref} \quad u'_{b,ref} \quad u'_{c,ref}]^{\mathrm{T}} = \left[\frac{(3u_{a,ref} - u_{\mathrm{dc}})}{2} \quad -\frac{u_{\mathrm{dc}}}{2} \quad 0\right]^{\mathrm{T}}. \tag{15}$$

Case II: $\boldsymbol{u_{ref}}$ is located in Hexagon I. The voltage vector is defined as $\boldsymbol{u_{ref\_1}}$, which is obtained by subtracting the center voltage vector ([1, 0, 0]) of Hexagon I from $\boldsymbol{u_{ref}}$. It can be expressed as

$$\begin{aligned} &[u_{a,ref\_1} \quad u_{b,ref\_1} \quad u_{c,ref\_1}]^{\mathrm{T}} \\ &= [u_{a,ref} \quad u_{b,ref} \quad u_{c,ref}]^{\mathrm{T}} - \left[\frac{u_{\mathrm{dc}}}{2} \quad 0 \quad 0\right]^{\mathrm{T}}. \end{aligned} \tag{16}$$

Obviously, $\boldsymbol{u_{ref\_1}}$ is located in Hexagon 0, as shown in Fig. 2, which satisfies the two-level modulation model. In order to reduce switching loss and output error in each control cycle at the same time, the two phases should be clamped, and only one phase should be modulated. This means that $\boldsymbol{u_{ref\_1}}$ is replaced by the vector $\boldsymbol{u'_{ref\_1}}$ that is the closest to $\boldsymbol{u_{ref\_1}}$ among the vectors at the edge of adjacent small triangle.

As shown in Fig. 3(b), assuming that the vector $\boldsymbol{u_{ref\_1}}$ is located in the triangle A1. The three sides of the triangle A1 are defined as l_1, l_2, and l_3, respectively. The vertical lines from the end vertex of the vector $\boldsymbol{u_{ref\_1}}$ to l_1, l_2, and l_3 are drawn with distances d_1, d_2, and d_3, respectively. The vectors connecting from the origin of the coordinates to the foot of perpendicular are $\boldsymbol{u'_{ref\_1\_1}}$, $\boldsymbol{u'_{ref\_1\_2}}$ and $\boldsymbol{u'_{ref\_1\_3}}$, respectively.

In the $\alpha\beta$ coordinates, the lines l_1, l_2, and l_3 and the distances d_1, d_2, and d_3 can be, respectively, expressed as

$$\begin{cases} l_1 : \sqrt{3}u_\alpha - u_\beta = 0, & d_1 = \left(\sqrt{3}u_\alpha - u_\beta\right)/2 \\ l_2 : \sqrt{3}u_\alpha + u_\beta - \sqrt{3} = 0, & d_2 = \left(\sqrt{3}u_\alpha + u_\beta - \sqrt{3}\right)/2 \\ l_3 : u_\beta = 0, & d_3 = u_\beta. \end{cases} \tag{17}$$

The vector $\boldsymbol{u_{ref\_1\_min}}$ corresponding to $d_{\min} = \min(d_1, d_2, d_3)$ is the closest vector to $\boldsymbol{u_{ref\_1}}$ among the vectors at the edge of adjacent small triangles. However, the vector $\boldsymbol{u_{ref\_1\_min}}$ is difficult to solve directly, but it can be expressed as the sum of two vectors

$$\boldsymbol{u'_{ref\_1}} = \boldsymbol{u'_{ref\_1\_min}} = \boldsymbol{u_{ref\_1}} + \boldsymbol{u_{err}} \tag{18}$$

where $\boldsymbol{u'_{ref\_1}}$ represents the actual output voltage vector under the two-level model when the proposed modulation method is adopted. Taking $\boldsymbol{u_{ref\_1}}$ closest to l_1 as an example, the error vector can be expressed as

$$\boldsymbol{u_{err}} = \frac{d_1}{\sqrt{3}}[-1 \quad 1 \quad 0]^{\mathrm{T}}. \tag{19}$$

According to the method in Case I, $\boldsymbol{u'_{ref\_1}}$ can be expressed as

$$[u'_{a,ref} \quad u'_{b,ref} \quad u'_{c,ref}]^{\mathrm{T}} = \left[0 \quad 0 \quad u_{c,ref} - \frac{u_{a,ref} + u_{b,ref}}{2}\right]^{\mathrm{T}}. \tag{20}$$

When $\boldsymbol{u_{ref}}_{\boldsymbol{1}}$ is located in the triangle A1, all the cases of $\boldsymbol{u'_{ref\_1}}$ are shown in Table II.

When $\boldsymbol{u_{ref}}$ is located in Hexagon I, the actual output voltage vector $\boldsymbol{u'_{ref}}$ is equal to $\boldsymbol{u'_{ref\_1}}$ add the center voltage vector subtracted from (16), $\boldsymbol{u'_{ref}}$ can be expressed as

$$\begin{aligned} &[u'_{a,ref} \quad u'_{b,ref} \quad u'_{c,ref}]^{\mathrm{T}} \\ &= [u'_{a,ref\_1} \quad u'_{b,ref\_1} \quad u'_{c,ref\_1}]^{\mathrm{T}} + \left[\frac{u_{\mathrm{dc}}}{2} \quad 0 \quad 0\right]^{\mathrm{T}}. \end{aligned} \tag{21}$$

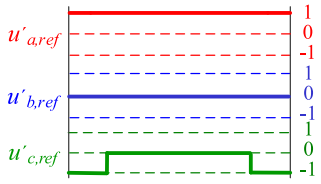

Fig. 4. Switching sequences of the proposed method.

B. Neutral Point Voltage Control of the Proposed Method

When the proposed method is adopted, two phases are clamped, and one phase is modulated in each control cycle. When $\boldsymbol{i}$ is in current state I, $\boldsymbol{u_{ref}}$ is in triangle A3, and $\boldsymbol{u_{ref}}_{\boldsymbol{1}}$ is closest to l_1, the switching sequences of the proposed modulation method are shown in Fig. 4.

Still taking the situation shown in Fig. 4 as an example, since phases A and B have been clamped, the current flowing into the neutral point can only be adjusted through phase C, which can be expressed as

$$\Delta i_{NP} = \Delta u \cdot \mathrm{sign}(i_c) \cdot \mathrm{sign}(-u'_{c,ref}) \tag{22}$$

where Δu represents the differential mode voltage injected into the modulated phase, and Δi_{NP} represents the neutral point current adjusted by Δu.

If $u_{C1} > u_{C2}$, the current flowing into the neutral point needs to be increased. At this time, $i_c < 0$, $u'_{c,ref} < 0$, phase C needs to be injected with a negative voltage to decrease the action time of level 0, as shown in Fig. 5(a). Conversely, if $u_{C1} \leq u_{C2}$, phase C needs to be injected with a positive voltage to decrease the action time of the 0 level, as shown in Fig. 5(b).

TABLE II
WHEN $\mathbf{u_{ref\_1}}$ IS LOCATED IN THE TRIANGLE A1, THE CALCULATION OF $\boldsymbol{u'_{ref\_1}}$

Location of $\boldsymbol{u}_{ref\_1}$	$\boldsymbol{u}'_{ref\_1}$ when $d_{\min}=d_1$	$\boldsymbol{u}'_{ref\_1}$ when $d_{\min}=d_2$	$\boldsymbol{u}'_{ref\_1}$ when $d_{\min}=d_3$
A1	$u'_{a,ref\_1}=0$	$u'_{a,ref\_1}=0$	$u'_{a,ref\_1}=u_{a,ref\_1}-\frac{u_{b,ref\_1}+u_{c,ref\_1}+u_{dc}}{2}$
	$u'_{b,ref\_1}=0$	$u'_{b,ref\_1}=u_{b,ref\_1}-\frac{(u_{a,ref\_1}+u_{c,ref\_1}+u_{dc})}{2}$	$u'_{b,ref\_1}=-\frac{u_{dc}}{2}$
	$u'_{c,ref\_1}=u_{c,ref\_1}-\frac{u_{a,ref\_1}+u_{b,ref\_1}}{2}$	$u'_{c,ref\_1}=-\frac{u_{dc}}{2}$	$u'_{c,ref\_1}=-\frac{u_{dc}}{2}$

In the $\alpha\beta$ coordinates, the lines l_1, l_2, and l_3 and the distances d_1, d_2, and d_3 can be, respectively, expressed as

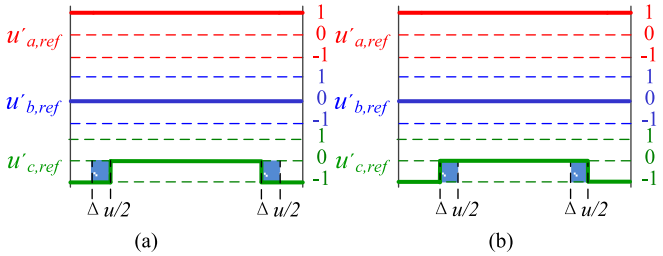

Fig. 5. Switching sequences with active neutral point voltage control. (a) $u_{C1}>u_{C2}$. (b) $u_{C1}\leq u_{C2}$.

In order to ensure that the injected differential mode voltage does not excessively increase the output error, Δu is limited to $0.05u_{\rm dc}$, and it is written as

$$\Delta u=\begin{cases}0.05u_{\rm dc}\\ k(u_{C1}-u_{C2})sign(-u'_{x,ref}\cdot i_x),-0.05u_{\rm dc}\\ <k(u_{C1}-u_{C2})<0.05u_{\rm dc}\\ -0.05u_{\rm dc}\end{cases} \tag{23}$$

where x represents the modulated phase and k is the proportional coefficient, which is related to the limitations of differential mode voltage and neutral point voltage fluctuation. In this article, the allowable neutral point voltage fluctuation is limited to $0.02u_{\rm dc}$, that is $-0.02u_{\rm dc}\leq u_{C1}\text{-}u_{C2}\leq 0.02u_{\rm dc}$. Then, k can be calculated as 2.5

$$k=\frac{0.05u_{\rm dc}}{0.02u_{\rm dc}}=2.5. \tag{24}$$

C. Algorithm Implementation of the Proposed Method

In summary, there are three steps to implement the proposed method. The first step is to predict $\boldsymbol{u}_{ref}$ by (6). The second step is to calculate $\boldsymbol{u'}_{ref}$ according to the method in Section IV. The third step is to calculate Δu_{NP} by (23) to control neutral point voltage. The specific implementation process of the proposed method is shown in Fig. 6, and the control block diagram of the system is shown in Fig. 7.

V. PERFORMANCE ANALYSIS

A. Switching Loss Analysis

The switching loss of SVPWM without current zero-crossing distortion processing, SVPWM with current zero-crossing distortion processing, CB-DSVM proposed in [15] and the proposed method in this article under different modulation index m are compared. The switching loss of SVPWM without current zero-crossing distortion processing is defined as the reference value, denoted as $P_{SL\_\rm SVPWM}$, then the switching loss of other modulation methods can be expressed as

$$P^*_{SL}=P_{SL}/P_{SL\_\rm SVPWM}. \tag{25}$$

The red, green, and blue colors in Fig. 8 represent the switching loss curves of SVPWM with current zero-crossing distortion processing, CB-DSVM and the proposed method, respectively. When SVPWM with current zero-crossing distortion processing is adopted, the output level of current zero-crossing phase is clamped to level 0 if the current is in the zero-crossing region; the modulation method is the same as that of SVPWM without current zero-crossing distortion if the current is not in the zero-crossing region. Therefore, the switching loss of this method is slightly better than that of SVPWM without current zero-crossing distortion processing. When CB-DSVM modulation is adopted by three-level rectifiers, the zero sequence voltage used to clamp a certain phase may change the sign of other phase voltages, which will cause current distortion and is not allowed in Vienna rectifier. Considering the abovementioned constraint, the phase with largest absolute value of the current may not be always clamped in each control cycle in Vienna rectifier. The lower the m is, the more constraints the clamping mode has. When m is less than 0.58, if CB-DSVM is adopted, only the phase with smallest absolute value of the current can be clamped, and the switching loss can be only reduced by 18%. Conversely, the higher the m is, the less constraints the clamping mode has. However, when m reaches the maximum value of 1.15, the clamping of the phase with largest absolute value of the current in each control cycle still cannot be guaranteed, and the reduction of switching loss is still less than 50% with CB-DSVM. There are always two phases clamped with the proposed method, which means that the reduction of switching loss is always greater than 50%. When m is around 0.58, the two phases corresponding to the maximum and medium absolute value of the current can be clamped in certain areas at the same time, and the switching loss can be reduced by 82%. When m reaches the maximum value of 1.15, the switching loss can still be reduced by 55%.

B. Output Error Analysis

When the proposed modulation method is adopted, the output error in a control cycle is the same every $\pi/3$. The output error under different m and ωt is shown in Fig. 9. The physical meaning

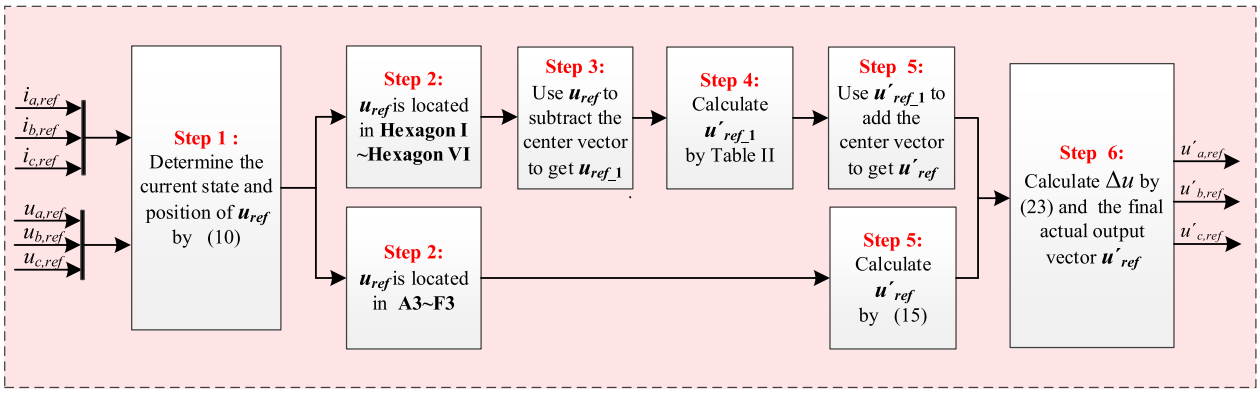

Fig. 6. Algorithm execution diagram of the proposed method.

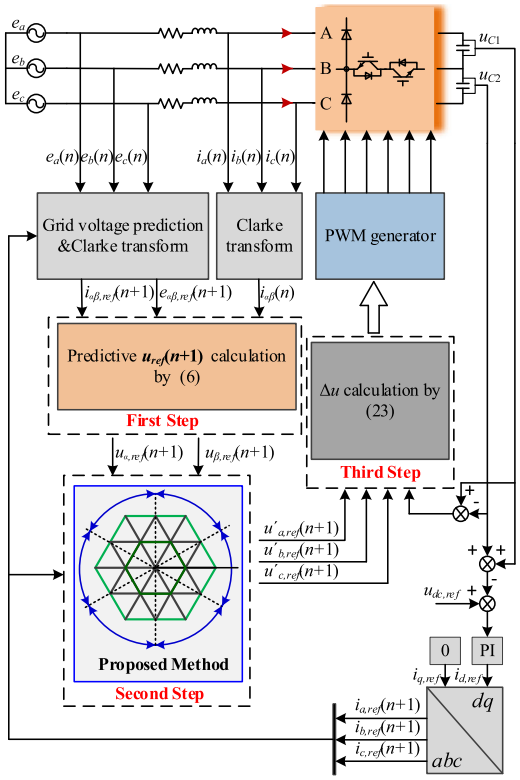

Fig. 7. Control block diagram adopted in this article.

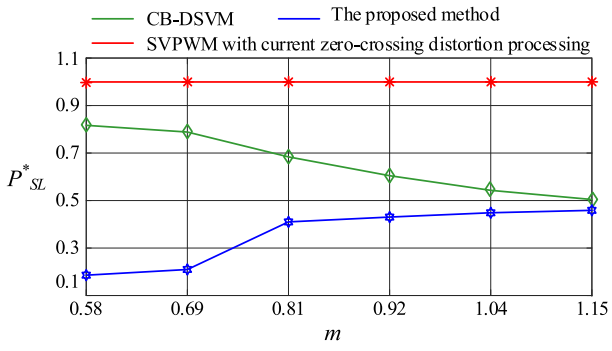

Fig. 8. Switching loss comparisons of different modulation methods.

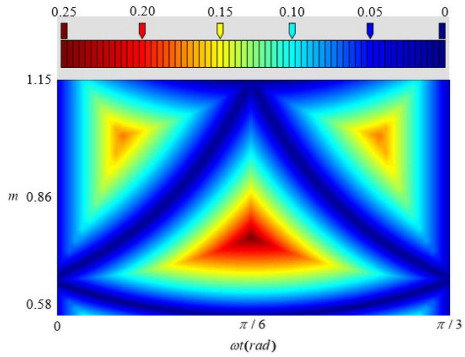

Fig. 9. Output error of the proposed method.

of the color in Fig. 9 is the ratio of the length of output error to that of u_{ref}.

It can be seen from Fig. 9 that the output error is less than 10% in most operating states. When m is near 0.58 and 1.15, the output error is almost zero; when m is 0.76 and ωt is $\pi/6$, the output error reaches the maximum value of 25%.

Based on the abovementioned analysis, the proposed method can reduce switching loss by more than 50% over the full range of m, and the output error is less than 10% in most operating regions. Especially when m is around 0.58, the switching loss can be reduced by 82%, and the output error is almost zero. If Vienna rectifier is operating with m around 0.58, the switching loss and current THD will be greatly reduced.

VI. Experimental Results

In order to verify the theoretical analysis, an experimental platform of Vienna rectifier was built, as shown in Fig. 10, and the main parameters of the system are shown in Table III.

SVPWM without current zero-crossing distortion processing, SVPWM with current zero-crossing distortion processing, CB-DSVM proposed in [15] and the proposed method in this article under different m are compared in terms of switching loss, efficiency and current THD. Figs. 11–13 are the experimental results of the four modulation methods with rated load when m is 0.60, 0.76, and 1.10, respectively. The dynamic experiments of the proposed method are also given in Figs. 14 and 15.

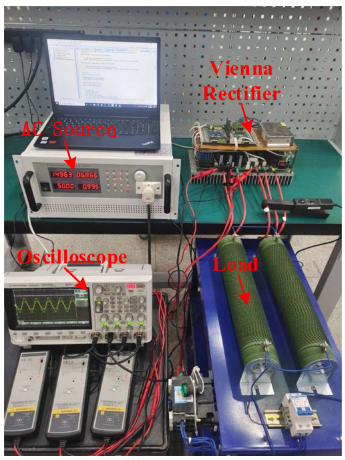

Fig. 10. Platform of the Vienna rectifier.

TABLE III
MAIN PARAMETERS OF THE SYSTEM

Parameter	Value
Dc-link voltage	450–550 V
upper and lower dc-link capacitor	1000 μF
grid voltage (rms)	116–213 V
input filter inductor	5 mH
carrier frequency	20 kHz
fundamental frequency	50 Hz

As shown in Figs. 11(a)–13(a), when SVPWM without current zero-crossing distortion processing is adopted, the current zero-crossing distortion is obvious over the full range of m, the fifth and seventh harmonics of the current are relatively high. In terms of current zero-crossing distortion, the effect of SVPWM with current zero-crossing distortion processing and CB-DSVM is similar. As shown in Figs. 11(b), 11(c), 12(b), and 12(c), in the range of medium and low m, the current zero-crossing distortion can be eliminated, and the fifth and seventh harmonics of the current are significantly reduced. As shown in Fig. 13(b) and 13(c), when m is very high, if the current is in the zero-crossing region, $\boldsymbol{u}_{ref}$ may not be accurately synthesized by any modulation method. The suppression effect of SVPWM with current zero-crossing distortion processing and CB-DSVM on current zero-crossing distortion is not obvious. For CB-DSVM, there is relatively large neutral point voltage fluctuation with triple fundamental frequency, which will lead to even order harmonics in phase current. Therefore, the current THD of CB-DSVM is always larger than that of SVPWM with current zero-crossing distortion processing. As shown in Figs. 11(d) and 12(d), in the range of medium and low m, when the proposed method is adopted, the current zero-crossing distortion can be eliminated, and the fifth and seventh harmonics of the current are significantly reduced. As shown in Fig. 13(d), in the range of very high m, when the proposed method is adopted, the current zero-crossing distortion can be minimized, and the fifth and seventh harmonics of the current are significantly lower than that of CB-DSVM and SVPWM with current zero-crossing distortion processing.

The current THDs of different modulation methods under different m and cut-off frequencies are listed in Table IV. It can be seen from Table IV that the current THDs of the latter three modulation methods are significantly better than that of SVPWM method without current zero-crossing distortion. When m is 0.60, the output error of the proposed method is low, and there is almost no neutral point voltage fluctuation with triple fundamental frequency. In terms of current THD with cut-off frequency of 2.5 kHz, the proposed method is almost the same as SVPWM with zero-crossing processing, and it is better than CB-DSVM. In terms of current THD with cut-off frequency of 30 kHz, the proposed method is worse than SVPWM with zero-crossing processing, but it is slightly better than CB-DSVM. When m is 0.76, the output error of the method proposed reaches the maximum. In terms of current THD with cut-off frequency of 2.5 kHz, the proposed method is almost the same as CB-DSVM, but it is worse than SVPWM with zero-crossing processing. In terms of current THD with cut-off frequency of 30 kHz, the proposed method is worse than SVPWM with zero-crossing processing and CB-DSVM. When m is 1.10, if the current is in the zero-crossing region, $\boldsymbol{u}_{ref}$ may not be accurately synthesized by any modulation method. The suppression effect of SVPWM with zero-crossing processing and CB-DSVM on current zero-crossing distortion is not obvious. In terms of current THD with cut-off frequency of 2.5 kHz, the proposed method is better than SVPWM with zero-crossing processing and CB-DSVM. That is because the proposed method is based on the principle of minimum output error. In terms of current THD with cut-off frequency of 30 kHz, the proposed method is slightly worse than SVPWM with zero-crossing processing, and it is slightly better than CB-DSVM.

Figs. 14 and 15 are the dynamic experimental results of the proposed method under step-up and step-down changes of load and dc-link voltage. It can be seen that the Vienna rectifier can still operate stably in the dynamic process with the proposed method. The dynamic response speed mainly depends on the control loop. In fact, the control loop of the proposed modulation method has no obvious improvement, and the dynamic experimental effect is almost the same as that of the other methods, which are not provided.

The switching loss and efficiency of different modulation methods are given in Table V and Fig. 16, respectively. For switching loss measurement, the adopted method in this article is the same as that in [23].

It can be seen that proposed method is better than the other three methods in terms of switching loss reduction. When SVPWM without current zero-crossing distortion processing is adopted, there are three switching actions in each control cycle for three phases, and the switching losses are large. Therefore, the efficiency of this method is lowest. When SVPWM with current zero-crossing distortion processing is adopted, the phase whose current is in the zero-crossing region is clamped to neutral point; if there is no current in the zero-crossing region, it is the same with SVPWM without current zero-crossing distortion. Therefore, the efficiency of SVPWM with current zero-crossing distortion processing is slightly higher than that without current zero-crossing distortion processing. When CB-DSVM is

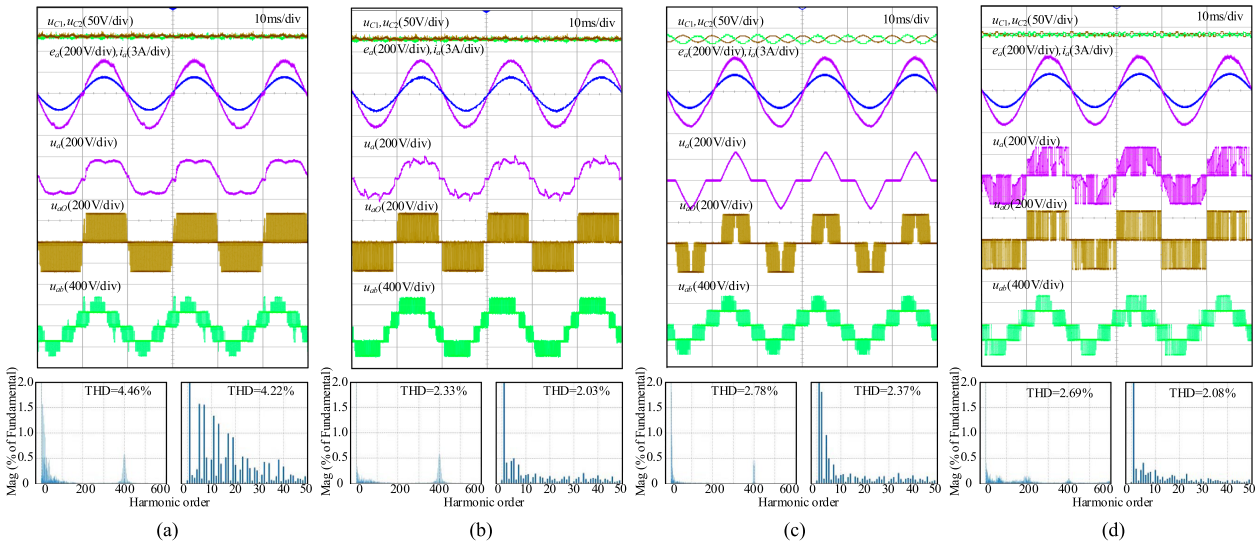

Fig. 11. Experimental results and current harmonic spectrums with different modulation methods. $m = 0.60$, $E = 116$V, $R_L = 235\Omega$, $u_{\rm dc} = 550$ V. (a) SVPWM without current zero-crossing distortion processing. (b) SVPWM with current zero-crossing distortion processing. (c) CB-DSVM. (d) Proposed method.

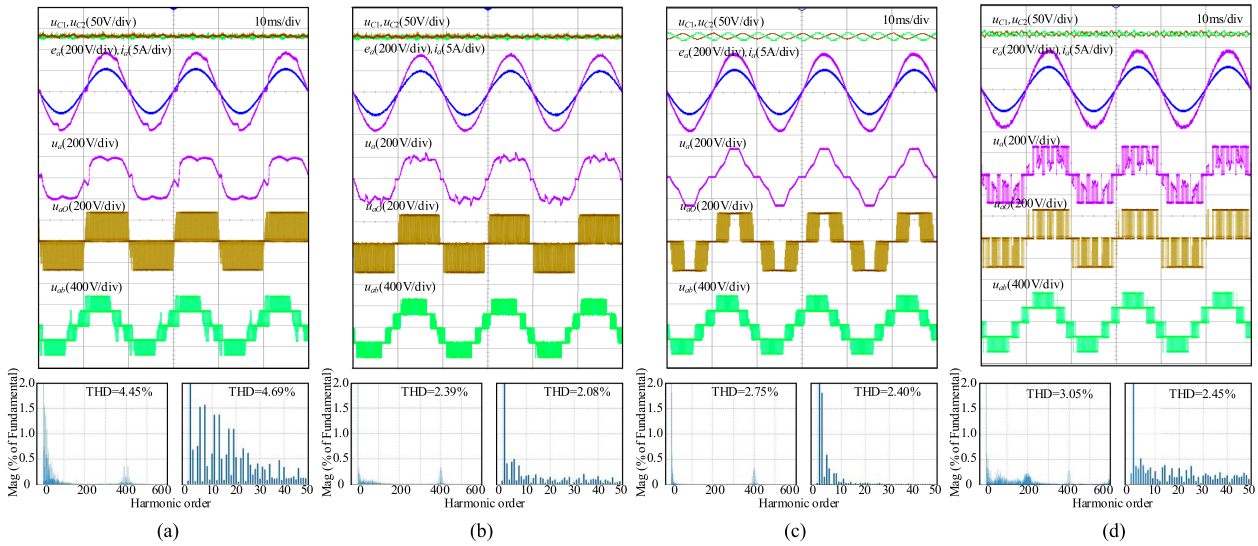

Fig. 12. Experimental results and current harmonic spectrums with different modulation methods. $m = 0.76$, $E = 150$ V, $R_L = 140\,\Omega$, $u_{\rm dc} = 550$ V. (a) SVPWM without current zero-crossing distortion processing. (b) SVPWM with current zero-crossing distortion processing. (c) CB-DSVM. (d) Proposed method.

TABLE IV
CURRENT THDS OF DIFFERENT MODULATION METHODS UNDER DIFFERENT M AND CUT-OFF FREQUENCIES

m	Cut-off frequency of FFT	SVPWM without current zero-crossing distortion processing	SVPWM with current zero-crossing distortion processing	CB-DSVM	The proposed method
0.60	2.5 kHz	4.22%	2.03%	2.37%	2.08%
	30 kHz	4.46%	2.33%	2.78%	2.69%
0.76	2.5 kHz	4.45%	2.08%	2.40%	2.45%
	30 kHz	4.69%	2.39%	2.75%	3.05%
1.10	2.5 kHz	4.78%	2.76%	2.91%	2.56%
	30 kHz	4.99%	3.08%	3.22%	3.17%

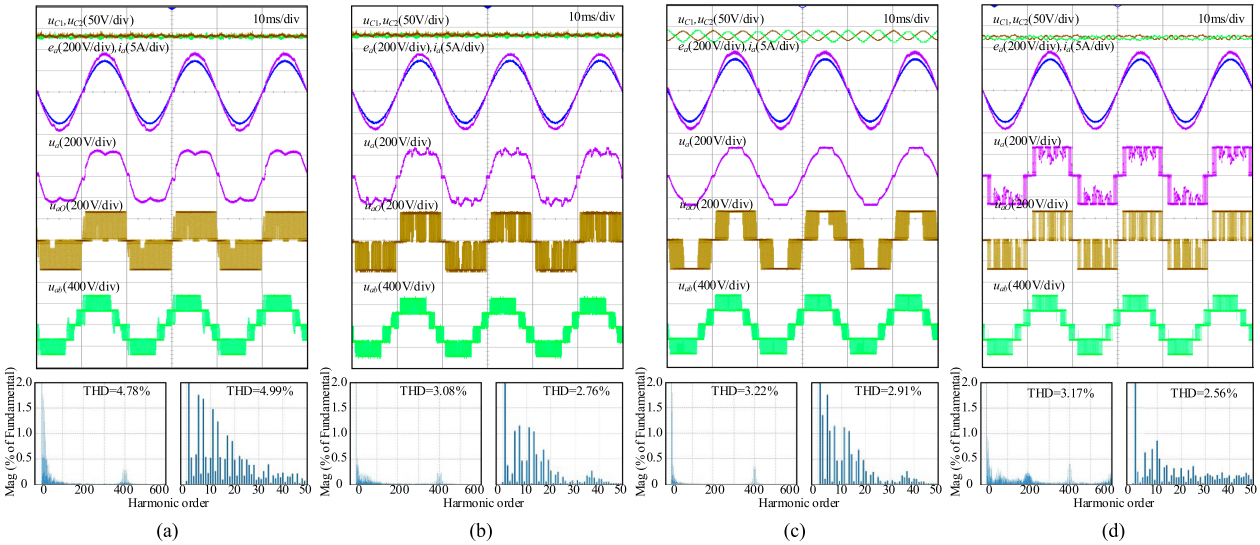

Fig. 13. Experimental results and current harmonic spectrums with different modulation methods. $m = 1.10$, $E = 213$V, $R_L = 70\ \Omega$, $u_{\rm dc} = 550$ V. (a) SVPWM without current zero-crossing distortion processing. (b) SVPWM with current zero-crossing distortion processing. (c) CB-DSVM. (d) Proposed method.

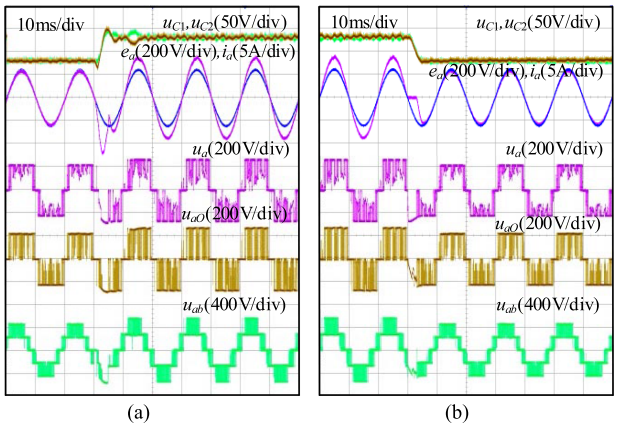

Fig. 14. Dynamic results of the proposed method under DC-link voltage step-up and step-down conditions. $E = 168$ V, $R_L = 100\ \Omega$. (a) DC-link voltage step-up from 450 to 550 V. (b) DC-link voltage step-down from 550 to 450 V.

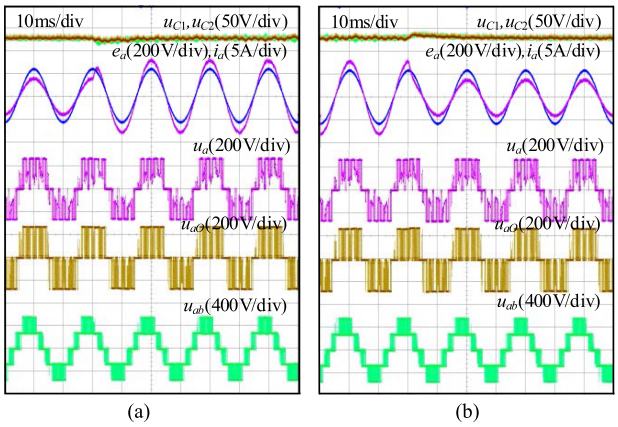

Fig. 15. Dynamic waveforms of the proposed method under load step-up and step-down conditions. $m = 0.86$, $E = 168$ V, $u_{\rm dc} = 550$ V. (a) R_L step-down from 200 to 100 Ω. (b) R_L step-up from 100 to 200 Ω.

TABLE V
EFFICIENCY UNDER OPERATING CONDITIONS OF FIGS. 11–13

	Fig. 11	Fig. 12	Fig. 13
SVPWM without current zero-crossing distortion processing	96.86%	97.00%	97.00%
SVPWM with current zero-crossing distortion processing	96.90%	97.11%	97.11%
CB-DSVM	97.30%	97.55%	97.70%
The proposed method	98.46%	98.03%	97.82%

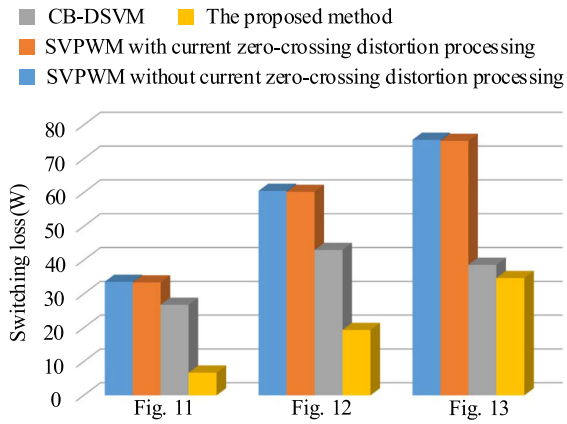

Fig. 16. Switching losses under operating conditions of Figs. 11–13.

adopted, one phase is always clamped and two phases are modulated. Therefore, the efficiency is significantly higher than that of the first two methods. With the increase of m, the interval of the clamped phase with largest absolute current gradually increases as well as its efficiency. When the proposed method is adopted, one phase is modulated and two phases are clamped. Therefore, its efficiency is significantly higher than that of the first three

methods. With the increase of m, the interval of the modulated phase with largest absolute current gradually increases, and its efficiency decreases.

VII. Conclusion

In this article, the voltage cost function is used to replace the current cost function, and $\boldsymbol{u}_{ref}$ used to accurately track the current is calculated. Then, the vectors at the edge of the triangle are selected as candidate vectors, and the vector closest to $\boldsymbol{u}_{ref}$ among the candidate vectors is selected as the output vector. If $\boldsymbol{u}_{ref}$ cannot be accurately synthesized by any modulation method, the method based on the principle of minimum synthesis error is given in this article, which is obviously better than the other existing methods in terms of current zero-crossing distortion caused by the fact that $\boldsymbol{u}_{ref}$ cannot be accurately synthesized. In addition, the three-phase output voltage is derived directly, which can greatly simplify the calculation. Finally, the neutral point voltage control method suitable for the method proposed is given. The superiority of the proposed method is verified by simulation and experimental results.

References

[1] X. Li et al., "A generalized design framework for neutral point voltage balance of three-phase Vienna rectifiers," *IEEE Trans. Power Electron* ., vol. 34, no. 10, pp. 10221–10232, Oct. 2019.

[2] T. Friedli, M. Hartmann, and J. W. Kolar, "The essence of three-phase PFC rectifier systems – Part II," *IEEE Trans. Power Electron* ., vol. 29, no. 2, pp. 543–560, Feb. 2014.

[3] A. Rajaei, M. Mohamadian, and A. Y. Varjani, "Vienna-rectifier-based direct torque control of PMSG for wind energy application," *IEEE Trans. Ind. Electron* ., vol. 60, no. 7, pp. 2919–2929, Jul. 2013.

[4] H. Chen and D. C. Aliprantis, "Analysis of squirrel-cage induction generator with VIENNA rectifier for wind energy conversion system," *IEEE Trans. Energy Convers.*, vol. 26, no. 3, pp. 967–975, Sep. 2011.

[5] J. Adhikari, P. IV, and S. K. Panda, "Reduction of input current harmonic distortions and balancing of output voltages of the Vienna rectifier under supply voltage disturbances," *IEEE Trans. Power Electron.*, vol. 32, no. 7, pp. 5802–5812, Jul. 2017.

[6] S. Yang, J.-H. Park, and K.-B. Lee, "Current quality improvement for a Vienna rectifier with high-switching frequency," *Trans. Korean Inst. Power Electron.*, vol. 22, no. 2, pp. 181–184, Apr. 2017.

[7] A. Ghaderi, T. Umeno, Y. Amano, and S. Masaru, "A novel seamless direct torque control for electric drive vehicles," *J. Power Electron.*, vol. 11, no. 4, pp. 449–455, Jul. 2011.

[8] S. Xu, J. Zhang, Y. Huang, and J. Jatskevich, "Dynamic average-value modeling of three-level T-Type grid-connected converter system," *IEEE J. Emerg. Sel. Topics Power Electron.*, vol. 7, no. 4, pp. 2428–2442, Dec. 2019.

[9] R. Davoodnezhad, D. G. Holmes, and B. P. McGrath, "A novel three level hysteresis current regulation strategy for three-phase three-level inverters," *IEEE Trans. Power Electron* ., vol. 29, no. 11, pp. 6100–6109, Nov. 2014.

[10] Y. D. Kwon, J. H. Park, K. M. Kim, and K. -B. Lee, "Line current improvement of three-phase four-wire VIENNA rectifier using dead beat control," in *Proc. IEEE Conf. Energy Convers.*, 2017, pp. 49–54.

[11] D. Tong, X. Y. Ren, Y. Chen, M. Xu, and Z. Hao, "A non-linear control strategy to reduce DC bus capacitance in Vienna rectifier," in *Proc. IEEE Appl. Power Electron. Conf. Expo.*, 2019, pp. 1776–1781.

[12] X. Li, S. Yao, H. Wang, M. Su, and S. Huang, "A hybrid control scheme for three-phase VIENNA rectifiers," *IEEE Trans. Power Electron.*, vol. 33, no. 1, pp. 629–640, Jan. 2018.

[13] J. -S. Lee, K. -B. Lee, and F. Blaabjerg, "Predictive control with discrete space-vector modulation of Vienna rectifier for driving PMSG of wind turbine systems," *IEEE Trans. Power Electron.*, vol. 34, no. 12, pp. 12368–12383, Dec. 2019.

[14] C. Dang et al., "Cost function-based modulation scheme of model predictive control for VIENNA rectifier," *IET Power Electron.*, vol. 12, no. 14, pp. 3646–3655, May 2019.

[15] Q. Wang et al., "A low-complexity optimal switching time-modulated model-predictive control for PMSM with three-level NPC converter," *IEEE Trans. Transp. Electrific.*, vol. 6, no. 3, pp. 1188–1198, Sep. 2020.

[16] Y. Yang, H. Wen, M. Fan, M. Xie, and R. Chen, "Fast finite-switching-state model predictive control method without weighting factors for T-Type three-level three-phase inverters," *IEEE Trans. Ind. Inform.*, vol. 15, no. 3, pp. 1298–1310, Mar. 2019.

[17] W. Zhu, C. Chen, S. Duan, T. Wang, and P. Liu, "A carrier-based discontinuous PWM method with varying clamped area for Vienna rectifier," *IEEE Trans. Ind. Electron.*, vol. 66, no. 9, pp. 7177–7188, Sep. 2019.

[18] J. Lee and K. Lee, "Performance analysis of carrier-based discontinuous PWM method for vienna rectifiers with neutral-point voltage balance," *IEEE Trans. Power Electron.*, vol. 31, no. 6, pp. 4075–4084, Jun. 2016.

[19] J. Wang, Y. Gao, and W. Jiang, "A carrier-based implementation of virtual space vector modulation for neutral-point-clamped three-level inverter," *IEEE Trans. Ind. Electron.*, vol. 64, no. 12, pp. 9580–9586, Dec. 2017.

[20] X. Li, Y. Sun, H. Wang, M. Su, and S. Huang, "A hybrid control scheme for three-phase vienna rectifiers," *IEEE Trans. Power Electron.*, vol. 33, no. 1, pp. 629–664, Jan. 2018.

[21] W. Alhosaini, F. Diao, M. H. Mahmud, Y. Wu, and Y. Zhao, "A virtual space vector-based model predictive control for inherent DC-link voltage balancing of three-level T-type converters," *IEEE J. Emerg. Sel. Topics Power Electron.*, vol. 9, no. 2, pp. 1751–1764, Apr. 2021.

[22] W. Jiang, X. Ding, Y. Ni, J. Wang, L. Wang, and W. Ma, "An improved deadbeat control for a three-phase three-line active power filter with current-tracking error compensation," *IEEE Trans. Power Electron.*, vol. 33, no. 3, pp. 2061–2072, Mar. 2018.

[23] W. Jiang, H. Jiang, S. Liu, S. Ji, and J. Wang, "A carrier-based discontinuous PWM strategy for T-type three-level converter with reduced common mode voltage, switching loss, and neutral point voltage control," *IEEE Trans. Power Electron.*, vol. 37, no. 2, pp. 1761–1771, Feb. 2022.

Qingyan Zhang was born in Shandong, China, in 1995. He received the B.S. degree in electrical engineering from the School of Electrical Engineering and Automation, Qufu Normal University, Rizhao, China, in 2018, and the M.S. degree in electrical engineering from School Electrical Engineering and Automation, Hefei University of Technology, Hefei, China, where he is currently working toward the Ph.D. degree in electrical engineering.

His main research interests include power electronics, and power converters in renewable energy.

Fang Liu (Senior Member, IEEE) was born in Shandong, China, in 1980. She received the B.S. M.S., and Ph.D. degrees in electrical engineering from the Hefei University of Technology, Hefei, China, in 2005, 2008, and 2015, respectively.

In 2015, she was the Teaching Faculty with the School of Electrical Engineering and Automation, Hefei University of Technology. She is currently an Associate Professor with the School of Electric Engineering and Automation, Hefei University of Technology, Hefei, China. From April 2008 to August 2009, she was a Software Engineer with EMERSON network Xian Power. From October 2011 to 2012, she was a Visiting Scholar with the Lab of WEMPEC, University of Wisconsin, Madison, WI, USA. Her research interests include the control and stability of renewable energy power system and power electronic conversion and application.

Weidong Jiang (Member, IEEE) was born in Sichuan, China, in 1976. He received the B.S. and Ph.D. degrees in electrical engineering from Hefei university of Technology, Hefei, China, in 1999 and 2004, respectively.

Since June 2004, he has been with the School of Electrical Engineering and Automation, Hefei University of Technology, Hefei, China, where he is currently a Professor. His research interests include electrical machines and their control systems, power electronics, and electric drives.

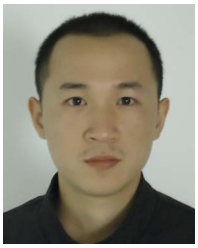

Jinping Wang (Member, IEEE) was born in Hunan, China, in 1984. He received the B.S. degree in electronic and information engineering and the Ph.D. degree in electrical engineering from Southwest Jiaotong University, Chengdu, China, in 2007 and 2013, respectively.

Since June 2013, he has been with the School of Electrical Engineering and Automation, Hefei University of Technology, Hefei, China, where he is currently an Associate Professor. His main research interests include modeling, analysis, control, and applications of switching-mode power supplies.

Yimin Yue was born in Hunan, China, in 1998. He received the B.S. degree in electrical engineering in 2020 from the School of Electrical Engineering and Automation, University of South China, Hengyang, China, where he is currently working toward the M.S. degree in electrical engineering with the School of Electrical Engineering and Automation, Hefei University of Technology, Hefei, China.

His main research interests include power electronics, and power converters in renewable energy.